Hopping at the resonance frequency: A trajectory generation technique for bipedal robots with elastic joints

Conference Paper *in* Proceedings - IEEE International Conference on Robotics and Automation · May 2012

DOI: 10.1109/ICRA.2012.6224909

4 authors, including:

Barkan Ugurlu
Ozyegin University
33 PUBLICATIONS **230** CITATIONS
SEE PROFILE

J.A. Saglia
Istituto Italiano di Tecnologia
19 PUBLICATIONS **292** CITATIONS
SEE PROFILE

Nikos G Tsagarakis
Istituto Italiano di Tecnologia
275 PUBLICATIONS **3,386** CITATIONS
SEE PROFILE

Hopping at the Resonance Frequency: A Trajectory Generation Technique for Bipedal Robots with Elastic Joints

Barkan Ugurlu, Jody A. Saglia, Nikos G. Tsagarakis, and Darwin G. Caldwell

***Abstract*— It is known that bipedal robots with passive compliant structures have obvious advantages over stiff robots, as they are able to handle the potential energy management. Therefore, this paper is aimed at presenting a jumping pattern generation method that takes advantage of this property via the utilization of the base resonance frequency, which is of special importance. To begin with, the resonance frequency is determined through a system identification procedure on our actual robot. Consequentially, the vertical component of the CoM is generated via a periodic function in which the resonance frequency is employed. The horizontal component of the CoM is obtained using the ZMP criterion to guarantee the dynamic balance. Having obtained the necessary elements of the CoM trajectory within an analytical manner, joint motions are computed with the help of translational and angular momenta constraints. In order to validate the method, two legged jumping experiments are conducted on our actual compliant robot. In conclusion, we observed repetitive, continuous, and dynamically equilibrated jumping cycles with feasible landing phases.**

I. Introduction

Contemporary humanoid robots appear to be the outcome of an impressive robotic evaluation, as they are able to perform almost-human-like versatile motion primitives. Back in 80s and 90s, the *dynamic walking* concept seemed a tough challenge; however, at the present time, not only dynamic walking but even jumping and running motions are already considered to be *fundamental* functions for humanoids.

Despite the dazzling robotic-evaluation, researchers still have second thoughts about the idea of having humanoids mingled in a dynamic human society [1]. Their hesitation is based on the fact that most humanoid robots are powered via stiff actuation modules with high gain servo controllers. The lack of compliance in these systems prevents us to constitute a safe human-robot co-existence. Furthermore, safety is not the only issue being compromised with these robots. Because of their stiff characteristics, they are not able to make use of natural dynamics and storage of energy during cyclic motions. Consequently, they have inherent shortcomings in dealing with the elastic potential energy management and environmental interactions.

Biological systems, on the other hand, have a smooth control over the elastic potential energy manipulation, as they store and release energy into/from their muscles and tendons during walking and running [2] [3]. This feature attracted many researchers in the field of biomechanics, to investigate compliance in legged locomotion. In [3], Ishikawa et al. stressed the importance of elastic energy usage in human walking. The coupling between forward velocity and stiffness is exploited in [4]. Resonance frequency phenomenon during human hopping is examined in [5] by Blickhan.

Being a basic requirement of running motion, legged jumping is also studied by roboticists from the trajectory and control synthesis point of view [6]–[9]. In these works, researchers prioritized dynamic balance and feasible/stable trajectories over the compliance issue. Sakka and Yokoi simulated vertical humanoid jumping with force feedback, to address force optimization issue [10]. Nevertheless, passive compliance could not be characterized in [6]–[10], as the actual or simulated robots are powered via stiff actuators.

In response to that matter, pneumatic artificial muscles are developed as a new actuation technology. Designating an antagonistic setup, Vanderborght et al. conducted walking and jumping experiments on a planar bipedal robot [11]. Hosoda and his students also adopted a similar strategy with a 3-D robot that is actuated by McKibben artificial muscles [12]. Regardless of their several advantages, pneumatic actuation has its own weak points. For instance, energy autonomy and power requirements still possess further challenges [13]. Furthermore, pneumatic actuation is argued to be not adequate in providing versatile maneuvering abilities required for humanoid locomotion.

Considering these factors, we developed a humanoid with SEA-based (Series Elastic Actuators) electrically actuated joints [14] [18], as a part of the European AMARSi project [15].The main objective of the AMARSi project is to succeed in a qualitative leap towards versatile motion skills in robotic systems, rigorously following a systematic approach in novel mechanical systems with compliance. Efficient jumping and running motion is listed one of these objectives as passive compliant actuators are expected to be advantageous in exploring fast motion generation methodologies.

In spite of the fact that researchers successfully demonstrated jumping motions on robots with artificial muscles [11] [12], a systematic pattern generation method is still lacking for a wider class of passively compliant humanoid robots. That being the case, this paper is aimed at proposing a possible solution for this problem. In our method, we utilized the base resonance frequency to generate z-axis CoM trajectory. The horizontal component of CoM is determined via the ZMP (Zero Moment Point) concept. Furthermore, initial conditions are tuned in a way to synthesize dynamically consistent jumping patterns. In doing so, the method appears to be systematic and easily applicable to wider class

B. Ugurlu is with the Control Systems Laboratory, Toyota Technological Institute, 2-12-1 Hisakata, Tempaku, Nagoya 468-8511, Japan. J. A. Saglia, N. G. Tsagarakis, and D. G. Caldwell are with the Department of Advanced Robotics, Istituto Italiano di Tecnologia, via Morego 30, Genova 16163, Italy. e-mail: nikos.tsagarakis@iit.it

TABLE I

MECHANICAL SPECIFICATIONS

Size	Upper Leg length: 226.63 [mm] Lower Leg length: 203.3 [mm] Ankle-sole length: 60.3 [mm]
Weight	Each Leg: 6.816 [kg] Waist: 4.41 [kg] Total : 17.772 [kg]

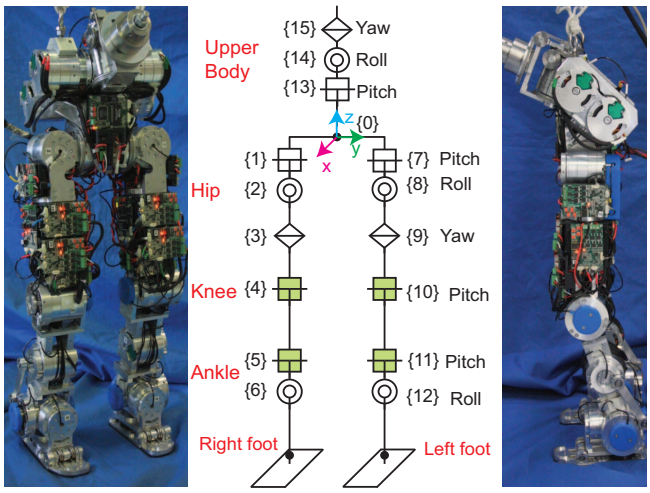

Fig. 1. The mechanical assembly of our robot and its joint configuration. The joints with light green color include passive compliant elements.

of passively compliant legged robots. Last but not least, this paper also reports one of a few jumping experimental results in which the resonance frequency is exploited. Similar approaches are also proposed for passive bipeds [16] and quadruped robots [17].

This paper is organized as follows. In section II, we briefly introduce our compliant bipedal robot. Jumping motion generation method is presented in section III. Experimental results are discussed thoroughly in section IV. Finally, the paper is concluded in section V by stating the remarks and addressing the future directions.

II. COMPLIANT BIPEDAL ROBOT

In order to explore compliant humanoid characteristics, we developed a bipedal robot in Italian Institute of Technology, as a part of AMARSi project. Table I summarizes its mechanical specifications. The robot has a total of 15 active DoF (degrees of freedom); 6 DoF in each leg, and 3 active DoF at the waist to be able to obtain greater motion flexibility. Each active joint incorporates three position sensors (two absolute and one relative encoders) to measure motor and link side angular positions. In addition, custom cell structure-based torque sensors are integrated to measure the actuator output torque. The robot is also equipped with 6-axis Force/Torque sensors at the ankles and five 1-axis load cells on the feet soles. In addition, it has a triaxial rate gyro sensor and an accelerometer, located at the pelvis. In its electronic hardware structure, the main controller is an Intel Core 2 Duo 1.5 GHz dual processor with 3.0 GB RAM, running on a 32-bit GNU/Linux operating system that includes real-time Xenomai extension. Data communication is performed via real-time Ethernet protocol called RTnet. Fig. 1 displays the actual robot and the joint configuration. For details, please refer to [18].

In this first prototype, only pitch axis ankle and knee joints are equipped with passive compliant elements, i.e., springs (see Fig. 1, light green joints). However, torque sensing and versatile position sensing elements are placed in all the joints to achieve active compliance.

III. JUMPING TRAJECTORY GENERATION

In the proposed approach, the main focus is to ascertain a jumping frequency to vertically excite the CoM, in a way to maximize the elastic potential energy storage. With this in mind, we performed a system identification routine on our actual bipedal robot to obtain such a feasible frequency (resonance frequency) within the range of physically realizable frequencies [5]. Having derived the vertical component of the CoM trajectory, the ZMP concept is employed for its horizontal counterpart. Successively, joint motions are computed using translational and angular momenta constraints. In this section, we disclose these procedures step by step.

As previously stated, only pitch axis ankle and knee joints are equipped with passive compliant elements in the current version of our bipedal robot. Because of this fact, we focus on two legged jumping motion generation, in which the robot moves on the sagittal plane, i.e., yaw axis and roll axis joint positions are set to zero. Only pitch axis hip, knee and ankle joints are activated. This postulate also enables us to give our full attention to generate jumping patterns on a relatively abstracted model. Note that we do not physically constraint the robot motion and it can move in the lateral plane if it is subject to an external force.

A. Determining the Resonance Frequencies

In our method, both legs move in an absolutely synchronized manner. Supposing that the friction between the feet soles and the floor is sufficient, we can consider the whole system as a multi-DoF rigid body-torsional spring system during support phases. Note that foot-ankle link does not move while the robot is in stance phase. Utilizing this model, it is possible to calculate two distinct resonance frequencies (δ_1, δ_2) which can be called the first (based) and second resonance frequencies.

On the other hand, theoretical computation of (δ_1, δ_2) might not provide sufficient precision for practical applications. Due to the compliance at the feet soles, harmonic gear stiffness, servo controller gains and several other factors, resonance frequencies may be diverged from their theoretical representations. In regard to this fact, we performed a system identification routine on our bipedal robot.

For this purpose, we firmly attached the robot feet to a rigid platform. Afterwards, the robot is excited through the vertical direction, using a chirp signal with frequencies ranging from 0.25 [Hz] to 8 [Hz]. Within this frequency range, we plotted angular deflections on both pitch axis

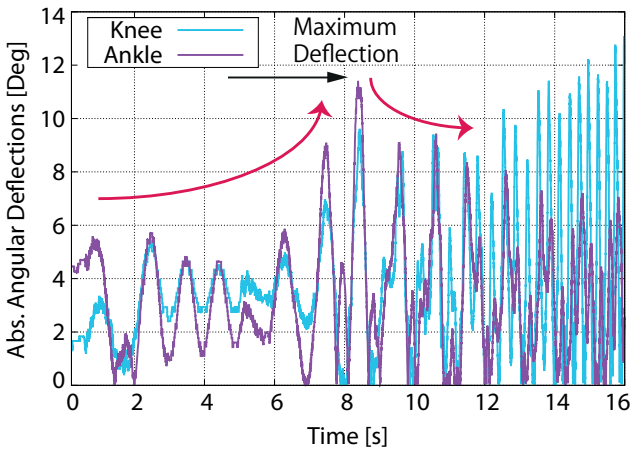

Fig. 2. System identification results on pitch axis ankle and knee joints. Angular deflections are measured on left leg's pitch axis ankle (solid purple) and knee (solid cyan) joints. Identical results are also obtained for the right leg. The actual experimentation period is longer than 16 [s]; however, the data after the 16^{th} second is truncated to display the worthwhile portion.

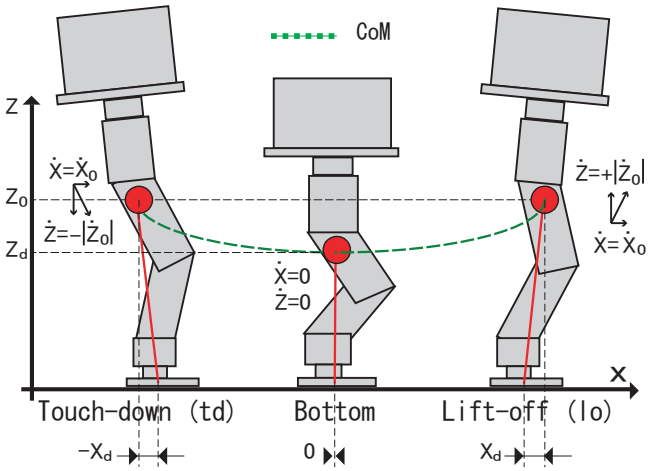

Fig. 3. Illustration of a single support phase period. It includes three main phases; a) Touch-down (from the previous flight phase), b) Bottom, c) Lift-off (for the next flight phase). Elastic potential energy is stored during touch-down - bottom period and then released throughout bottom - lift-off period. During support phases, the foot is stationary and its center is considered to be the origin. The offsets in x-axis are solely left for illustrative purposes. Since the foot sole center is substituted as origin, the CoM trajectory is determined with respect to this point. In order to prevent slips, we placed pads at the feet soles and did not consider large forward velocities.

ankle and knee joints as in Fig. 2, and sought for maximum deflections.

As observed in Fig. 2, both angular deflections reach to the maximum value slightly after the 8^{th} second. This corresponds to a frequency value of 0.845 [Hz]; namely, the base resonance frequency (δ_1). In this matter, our theoretical computation returned 1.1205 [Hz], which is within the vicinity of the experimentally obtained value but not precise enough. Furthermore, frequencies greater than δ_1 created gradually decreasing angular deflections as well. Consequently, we obtain a profile that is similar to a Gaussian distribution.

Our computations indicate that the second resonance frequency (δ_2) is around 10 [Hz], which is not within the physically feasible frequency range. Considering this fact, we choose to excite the robot body using δ_1. What is more, both joint deflections are simultaneously reach their maximum values when the frequency is at δ_1. Due to this outcome, we can hypothetically maximize the elastic potential energy storage.

B. CoM Trajectory Generation During Support Phase

For the CoM motion generation task during support phases, we make use of the ZMP concept. Primarily, let us analyze the x-axis ZMP equation [9].

$$X_{zmp} = x - \frac{\ddot{x}}{\ddot{z}+g} z - \frac{\dot{L}_y}{m(\ddot{z}+g)} \tag{1}$$

In (1), x, y and z symbolize CoM position, L_y is pitch axis intrinsic angular momentum, m is the total mass and g is the gravitational acceleration. Moreover, one dot and two dots denote first and second time derivatives. To simplify the motion generation task, $\dot{L}_y$ is omitted. We later include angular momentum information in joint computation stage.

Considering the aforementioned assumption, (1) may be rewritten as below.

$$\omega = \sqrt{\frac{\ddot{z}+g}{z}} \tag{2}$$

$$\ddot{x} = \omega^2 (x - X_{zmp}) \tag{3}$$

The ω parameter in (2) is called the natural frequency of the equivalent pendulum in ZMP modeling [8] [19]. The core idea is that if we equalize ω to the constant base resonance frequency (δ_1), we can maximize the elastic potential energy during jumping. Being second order differential equations, (2) and (3) can be analytically solved for constant ω values ($\omega = \delta_1$) to obtain the CoM trajectory. In following subsections, we explain this motion planning for vertical and horizontal components, respectively.

1) Vertical CoM Motion Planning: Eq. (2) can be written in a way to move the highest order to the left hand side.

$$\ddot{z} = \omega^2 z - g \tag{4}$$

For constant ω values, we may analytically solve (4) as in the following.

$$z = \left(z_0 - \frac{g}{\omega^2}\right)\cosh \omega t + \frac{\dot{z}_0}{\omega}\sinh \omega t + \frac{g}{\omega^2} \tag{5}$$

In (5), z_0 and $\dot{z}_0$ are initial position and velocity values, t is the time parameter. If we differentiate this equation, we can obtain the vertical CoM velocity as well.

$$\dot{z} = \left(\frac{\omega^2 z_0 - g}{\omega}\right)\sinh \omega t + \dot{z}_0 \cosh \omega t \tag{6}$$

At this stage, we would like to highlight the fact that the reason to obtain vertical CoM trajectory by solving (4) is to make sure that ω parameter is constant. As previously stated, our strategy is to generate a vertical CoM trajectory, excited with the constant natural frequency, i.e., the base resonance frequency (δ_1). This is due to the fact that the passive compliant joints in our robots have approximately fixed stiffness. Therefore, we are in need of vertical CoM patterns in which the natural frequency is constant as well. Consequently, this condition allowed us to yield (5) through the analytical solution of (4).

One may think that another periodic function could also be employed for the vertical CoM trajectory. However, in that scenario, (2) does not hold valid for constant ω values; it varies with time. Of course, variable stiffness actuators [20] might enable us to use various other vertical CoM patterns with varying ω values. On the other hand, these actuators are still large-sized and their adaptation to humanoid robotics is currently under development.

In order to obtain periodic elastic energy transformation routines using (5) and (6), it is desirable to obtain a vertical motion profile in which the robot moves downwards and upwards in a subsequent fashion. Together with Fig. 3; Fig. 4-(a) and Fig. 4-(b) depict this kind of vertical position and velocity profiles throughout the desired support period. As observed in these figures, the robot starts from an initial position, z_0, with a negative initial velocity, $-|\dot{z}_0|$, at the moment of t_0, then decelerate downwards. In the middle point of the support phase ($t = t_{mz}$), the CoM reaches to its minimum value, z_d. Between t_0 and t_{mz}, the springs store elastic potential energy. After the t_{mz} moment, the robot releases the elastic potential energy and accelerate upwards. It lifts off at the end of the support phase, t_e. Because the motion is symmetric, the vertical initial position equals to the vertical lift-off position. Moreover, the vertical initial and lift-off velocities have the same magnitude with different signs.

As noted by Blickhan [5], the number of independent parameters are less than constraints in jumping motion. Since constraints limit the parameter space where a feasible jump is possible, they must be well tuned to each other. In our method, we determine z_0 and z_d values by considering the mechanical capabilities of our robot. ω is equalized to the base resonance frequency as previously explained; $\omega = \delta_1$. Other parameters, namely initial velocity ($\dot{z}_0$) and support time period (T_s), are computed by using z_0, z_d and ω values to make sure that we obtain the motion profile shown in Fig. 4-(a) and Fig. 4-(b).

In Fig. 4-(a), we can observe that the vertical position function has a minimum when $t = t_{mz}$. In other words, the velocity function is zero at this moment. If we call support time period as T_s, and initial time (t_0) is zero[1], t_{mz} simply becomes $T_s/2$.

$$\dot{z}|_{t=T_s/2} = \frac{\omega^2 z_0 - g}{\omega} \sinh \omega \frac{Ts}{2} + \dot{z}_0 \cosh \omega \frac{Ts}{2} = 0 \qquad (7)$$

[1]For non-zero initial time values, resulting equations can simply be shifted in time through t_0, without the loss of generality.

From (7), T_s parameter can be expressed in terms of ω, z_0 and $\dot{z}_0$.

$$T_s = \frac{2}{\omega} \tanh^{-1} \frac{\dot{z}_0 \omega}{g - \omega^2 z_0} \qquad (8)$$

Additionally, the z-axis CoM position equals to z_d when $t = t_{mz} = T_s/2$.

$$\begin{aligned} z|_{t=T_s/2} &= \frac{\omega^2 z_0 - g}{\omega^2} \cosh \omega \frac{T_s}{2} \\ &+ \frac{\dot{z}_0}{\omega} \sinh \omega \frac{T_s}{2} + \frac{g}{\omega^2} = z_d \end{aligned} \qquad (9)$$

Combining (8) and (9), and solving the outcome for $\dot{z}_0$, the following relation is obtained.

$$\dot{z}_0 = \mp \sqrt{(z_0 - z_d)\left(\omega^2 z_0 - 2g + \omega^2 z_d\right)} \qquad (10)$$

Even though we have two solutions, we need to choose with the minus sign, in order to comply with the desired vertical motion profile.

Utilizing (10), we can compute the initial vertical CoM velocity, $\dot{z}_0$, for a given set of z_0, z_d and ω. Subsequently, we can compute the support time period, T_s, using (8). Inserting all these parameters into (5) and (6), vertical CoM position and velocity trajectories are yielded. To this end, we later provide a simple algorithm to generate trajectories.

2) Horizontal CoM Motion Planning: Having obtained the vertical CoM trajectory, we now follow a similar strategy for the horizontal CoM trajectory [14]. Keeping in mind that ω is constant and equals to δ_1, we can solve (3) for a constant X_{zmp} as below.

$$x = (x_0 - X_{zmp}) \cosh \omega t + \frac{\dot{x}_0}{\omega} \sinh \omega t + X_{zmp} \qquad (11)$$

Initial position and velocity are denoted with x_0 and $\dot{x}_0$. Differentiating (11) once and twice, we can obtain x-axis velocity and acceleration functions as well.

$$\dot{x} = \omega (x_0 - X_{zmp}) \sinh \omega t + \dot{x}_0 \cosh \omega t \qquad (12)$$

$$\ddot{x} = \omega^2 (x_0 - X_{zmp}) \cosh \omega t + \omega \dot{x}_0 \sinh \omega t. \qquad (13)$$

When there is a requirement to generate ZMP-based feasible x-axis CoM trajectories, it is desirable to obtain a motion profile in which the robot decelerates and accelerates within a consequent manner. In addition to Fig. 3, Fig. 4-(c) and Fig. 4-(d) depict the horizontal position and velocity profiles for this kind of trajectory generation. In these figures, the deceleration phase is defined between t_0 and t_{mx} while the acceleration phase is defined between t_{mx} and t_e. Depending on the desired deceleration/acceleration strategy, t_{mx} can be assigned between t_0 and t_e. In case of substituting t_{mx} as the middle point, deceleration/acceleration periods become equal to each other. The CoM then moves forward by keeping its average pace and its terminal velocity becomes equal to the initial velocity. Fig. 4-(c) and Fig. 4-(d) demonstrate such a

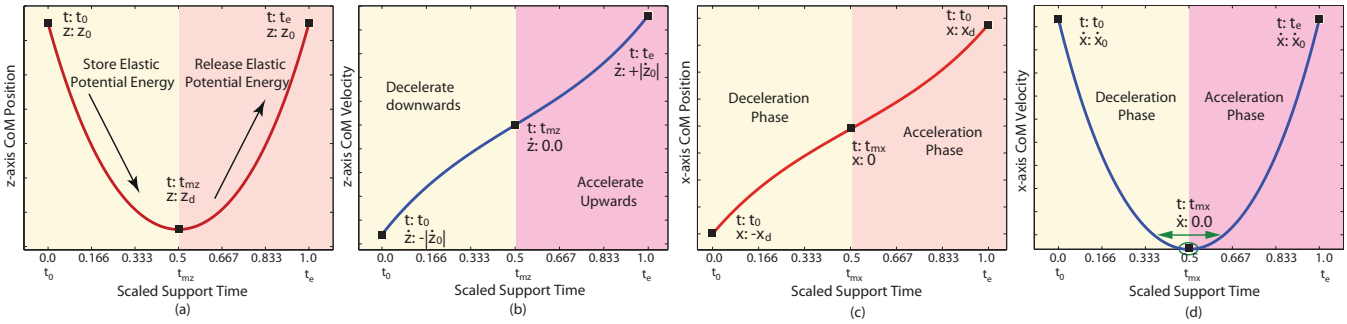

Fig. 4. Feasible CoM position and velocity profiles. a) z-axis CoM position. b) z-axis CoM velocity. c) x-axis CoM position. d) x-axis CoM velocity.

situation. Because the motion is symmetric, the horizontal initial velocity equals to the horizontal lift-off velocity.

As it may be observed in Fig. 4-(d), velocity function has a minimum point when $t = t_{mx}$. Hence, its derivative, the acceleration function is zero at that moment.

$$\begin{aligned} \ddot{x}|_{t=t_{mx}} &= \omega^2(x_0 - X_{zmp})\cosh\omega t_{mx} \\ &+ \omega\dot{x}_0 \sinh\omega t_{mx} = 0 \end{aligned} \tag{14}$$

Using (14), we can express $\dot{x}_0$ as follows.

$$\dot{x}_0 = \omega((X_{zmp} - x_0)\coth\omega t_{mx} \tag{15}$$

During single support phases, it is also possible to substitute an average forward velocity, υ_m. Assigning this parameter, the terminal position, x_d, can simply be obtained by the following formula.

$$x_d = \upsilon_m T_s + x_0. \tag{16}$$

In the case of cyclic motion, the x_0 parameter in (16) equals to the lift-off position with a minus sign ($-x_d$) as illustrated in Fig. 3. If the robot starts jumping from a stationary motion, i.e., the beginning of an experiment, it could be substituted as zero or a relatively small value.

The x_d parameter in (3) also corresponds to the position when $t{=}t_e$:

$$\begin{aligned} x|_{t=t_e} &= x_d = (x_0 - X_{zmp})\cosh\omega T_s \\ &+ \frac{\dot{x}_0}{\omega}\sinh\omega T_s + X_{zmp}. \end{aligned} \tag{17}$$

Inserting (15) and (16) into (17), we may compute X_{zmp}.

$$X_{zmp} = \frac{x_0\sinh(\omega(T_s - t_{mx})) + x_d\sinh(\omega t_{mx})}{\sinh(\omega(T_s - t_{mx})) + \sinh(\omega t_{mx})}. \tag{18}$$

In a basic sense, for a given set of x_0, ω, υ_m and t_{mx} profile, (16), (18), and (15) enables us to compute X_{zmp} and $\dot{x}_0$ parameters, respectively. Having obtained x_0, $\dot{x}_0$ and X_{zmp}, we can generate the horizontal CoM position and velocity trajectories by utilizing (11) and (12). On this matter, we later provide an easy-to-implement algorithm. A similar analytical pattern generation methodology with piecewise functions can be observed in [21] for bipedal walking.

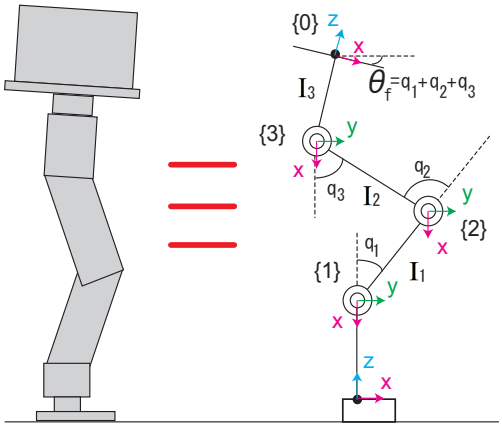

Fig. 5. Kinematic structure of our bipedal robot in the sagittal plane. Associated joint frames are indicated.

C. CoM Trajectory Generation During Flight Phase

In generating the CoM trajectory during flight phases, we adopted the method described in [9]. To explain briefly, we make use of projectile motion dynamics in which the x-axis translational and pitch axis angular momenta are conserved. As for z-axis motion, the CoM follows a parabola. x-axis and z-axis foot trajectories are also computed in a way to create a seamless connection between consecutive support and flight phases. Note that ZMP is undefined in this phase. For further details, please refer to [9].

D. Joint Computation Scheme

Having computed all the necessary components of CoM trajectories, we now proceed to joint computation scheme. As we stated previously, only the joints in sagittal plane are equipped with passive compliant elements. Therefore, we focus on jumping motion in which pitch axis ankle, knee and hip joints are actuated, i.e., 3 DoF. For this purpose, we consider a simplified bipedal robot model in which yaw axis and roll axis joint positions are set to zero. Moreover, corresponding pitch axis joints in right and left legs are always equal to each other. Hereby, left and right legs do move in a synchronized manner throughout jumping cycles. Fig. 5 displays our model and joint frames. Note that we do not physically constrain the robot motion and it can move in

the lateral plane if it is subject to external forces.

At this point, we can easily derive an analytical inverse kinematics solution that maps CoM position and upper body pitch axis orientation (x, z, θ_f) with joint positions (q). On the other hand, this approach cannot characterize the rotational inertia, an important characteristics of the robot dynamics. Considering this fact, we utilized x-axis and z-axis CoM translational momenta (P_x, P_z) and pitch axis CoM angular momentum (L_y). These momenta values can be computed in terms of joint velocities ($\dot{\mathbf{q}}$) as shown below.

$$P_x = mJ_{x1}\dot{q}_1 + mJ_{x2}\dot{q}_2 + mJ_{x3}\dot{q}_3 \quad (19)$$

$$P_z = mJ_{z1}\dot{q}_1 + mJ_{z2}\dot{q}_2 + mJ_{z3}\dot{q}_3 \quad (20)$$

$$L_y = \lambda\left(\begin{bmatrix} Fk_{xcom} & 0 & Fk_{zcom} \end{bmatrix}^T \times \begin{bmatrix} P_x & 0 & P_z \end{bmatrix}^T\right) + I_1\dot{q}_1 + I_2(\dot{q}_1+\dot{q}_2) + I_3(\dot{q}_1+\dot{q}_2+\dot{q}_3) \quad (21)$$

In (19), (20) and (21), Fk_{xcom} are Fk_{zcom} forward kinematics functions that map joint positions to x-axis and z-axis CoM position. $\lambda = [0\ 1\ 0]$ is a row vector to extract the second element of the outcome of the cross product. I_1, I_2 and I_3 are rotational inertia parameters associated with the sagittal plane. $\dot{q}_1$, $\dot{q}_1$ and $\dot{q}_3$ are ankle, knee and hip joint velocities. Corresponding parameters can be examined in Fig. 5. Moreover, J_{x1}, J_{x2}, J_{x3}, J_{z1}, J_{z2} and J_{z3} are Jacobian matrix elements which maps CoM translational velocity to joint velocities. They can be computed through partial differentiation.

$$J_{x1} = \frac{\partial Fk_{xcom}}{\partial q_1},\ J_{x2} = \frac{\partial Fk_{xcom}}{\partial q_2},\ J_{x3} = \frac{\partial Fk_{xcom}}{\partial q_3}, \quad (22)$$

$$J_{z1} = \frac{\partial Fk_{zcom}}{\partial q_1},\ J_{z2} = \frac{\partial Fk_{zcom}}{\partial q_2},\ J_{z3} = \frac{\partial Fk_{zcom}}{\partial q_3}. \quad (23)$$

We can rearrange (19), (20) and (21) in matrix form.

$$\overbrace{\begin{bmatrix} P_x \\ P_z \\ L_y \end{bmatrix}}^{\mathbf{H}} = \overbrace{\begin{bmatrix} mJ_{x1} & mJ_{x2} & mJ_{x3} \\ mJ_{z1} & mJ_{z2} & mJ_{z3} \\ \mu_1 & \mu_2 & \mu_3 \end{bmatrix}}^{M\ Matrix} \overbrace{\begin{bmatrix} \dot{q}_1 \\ \dot{q}_2 \\ \dot{q}_3 \end{bmatrix}}^{\dot{\mathbf{q}}} \quad (24)$$

In (24), following subexpressions are used.

$$\mu_1 = I_1+I_2+I_3+m(Fk_{zcom}J_{x1}-Fk_{xcom}J_{z1}) \quad (25)$$

$$\mu_2 = I_2+I_3+m(Fk_{zcom}J_{x2}-Fk_{xcom}J_{z2}) \quad (26)$$

$$\mu_3 = I_3+m(Fk_{zcom}J_{x3}-Fk_{xcom}J_{z3}) \quad (27)$$

Inverting the M matrix with proper algorithms that prevent error accumulation [22], we can compute joint velocities ($\dot{q}_1$, $\dot{q}_2$, $\dot{q}_3$), for a given set of total momenta (P_x, P_z, L_y).

$$\dot{\mathbf{q}} = M^{-1}\mathbf{H}. \quad (28)$$

Note that the M matrix is of full rank for all joint motion values except for the case of fully extended knee. $\mathbf{H}$, M, $\dot{\mathbf{q}}$ are indicated in (24). Having computed joint velocity references, we can easily obtain joint position references via a discrete integration procedure.

$$\mathbf{q}_{[k]} = \mathbf{q}_{[k-1]} + \frac{\Delta t}{2}\left(M^{-1}_{[k]}\mathbf{H}_{[k]} + M^{-1}_{[k-1]}\mathbf{H}_{[k-1]}\right) \quad (29)$$

In (29), k stands for the discrete event index. Δt is the sampling period. We can utilize (29) as long as $k > 0$. For the case of $k = 0$, $\mathbf{q}_{[0]}$ is supplied in advance. Having derived the joint position and velocity references using (28) and (29), we insert them into local servo blocks in which position and velocity control are applied to compute joint torques.

Keep in mind that the above calculations are adequate for planar systems and observed to be practically useful in the current work. For more general joint computation schemes with momenta constraints, refer to [6] and [8].

E. Trajectory Generation Algorithm

Evaluating the overall computations performed above, it is possible to construct an easy-to-follow algorithm for the bipedal jumping generation task as below. Note that calculations should be done in a sequential manner.

1) Determine the resonance frequency at which the robot will be vertically excited.
2) Substitute initial position values; x_0 and z_0.
3) Designate a z_d value by considering the joint ranges.
4) Assign υ_m and t_{mx} values by considering the forward deceleration/acceleration strategy.
5) Calculate $\dot{z}_0$ by using (10).
6) Calculate support time period, T_s, by using (8).
7) Calculate x_d using (16).
8) Calculate X_{zmp} using (18). If it is not within the support polygon boundaries, change the forward deceleration/acceleration strategy and re-compute.
9) Calculate $\dot{x}_0$ using (15).

If the robot is in support phase;

- Generate x-axis and z-axis CoM velocities by utilizing (12) and (6). Multiply them with total mass, m, to obtain P_x and P_z inputs.
- Designate the pitch axis angular momentum (L_y) profile.
- Generate joint position and velocity references by using (28) and (29). Apply these inputs to local servo units.

If the robot is in flight phase;

- Perform the CoM and foot pattern generation as described in [9].
- Generate joint position and velocity references by using (28) and (29). Apply these inputs to local servo units.

IV. Experimental Results and Discussions

In order to validate the proposed technique, we conducted two legged hopping experiments on our actual compliant robot. In these experiments, initial vertical and horizontal CoM positions (z_0, x_0), minimum vertical position (z_d), average velocity (υ_m), and flight time (T_f) are designated as 0.36 [m], 0.005 [m], 0.3 [m], 0.08 [m/s], and 0.15 [s] respectively. Other parameters are computed in accordance

with the algorithm. Results may be examined from Fig. 6 to Fig. 9.

Center of mass trajectories are depicted in Fig. 6, both for x-axis and z-axis. From these figures, we may observe that consecutive support and flight phases are connected seamlessly. Note that these CoM trajectories are computed with respect to foot sole center and therefore, x-axis trajectory seems periodic.

Vertical GRF (Ground Reaction Force) can be observed in Fig. 7-(a). In this figure, zero GRF response intervals indicate successful flight phases and these are colored with light yellow. Moreover, we may also examine the touch down impact which is about 350 [N]. A similar jumping experiment on a rigid robot with 25% less weight resulted as 600 [N] [9]. Based on this result, we may claim that robots with compliant joints have inherent capabilities in reducing the ground impacts.

Horizontal ZMP response is displayed in Fig. 7-(b). ZMP response is displayed with solid red line while the support polygon is symbolized with dot green and dot blue lines. Light yellow areas stand for flight phases in which the ZMP is undefined. Based on the fact that ZMP response is always within the support polygon; we obtained continuous and dynamically equilibrated jumping cycles.

To be able to clarify the effect of the resonance frequency, we also performed jumping experiments in which the vertical trajectory is generated using a frequency that is 25% larger than the resonance frequency; $\delta_q = 1.25\delta_1$. Let us call it non-resonant jumping. In Fig. 8, we may see ankle joint's spring deflections (a) and stored elastic potential energy (b), for both cases. Blue and green lines stand for the resonant (δ_1) and non-resonant (δ_q) frequency jumping experiment results, respectively.

From Fig. 8-(a), it is obvious that the measured deflection is about 2.5 times larger in the resonant jumping, comparing to the non-resonant case. Hence, it is possible to judge that the vertical trajectory that is generated at the resonance frequency is more advantageous over other cases in generating a jumping motion with larger displacements. Furthermore, the maximum deflection in resonant jumping is about -11.2 [Deg], which is almost the maximum allowable deflection (-11.45 [Deg]).

The stored elastic potential energy is calculated via integrating the multiplication of measured deflections with the stiffness over the interval. The results can be examined in Fig. 8-(b). As observed in this figure, the elastic potential energy is about 10 times larger in the resonant jumping than in the non-resonant jumping. This is one of the main results that illustrate the effectiveness of the utilization of resonance frequency in bipedal jumping motion. Note that non-resonant jumping experiment did not completely succeed; the robot demonstrated premature flight phases in which there were no obvious foot clearance.

We additionally would like to highlight the fact that it is not possible to demonstrate jumping motion on this robot without the passive compliance, due to the current hardware configuration.

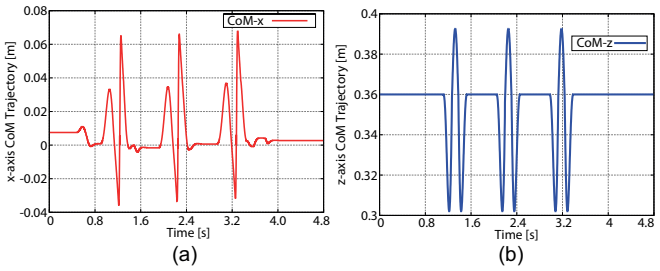

Fig. 6. CoM trajectories. a) x-axis, b) z-axis.

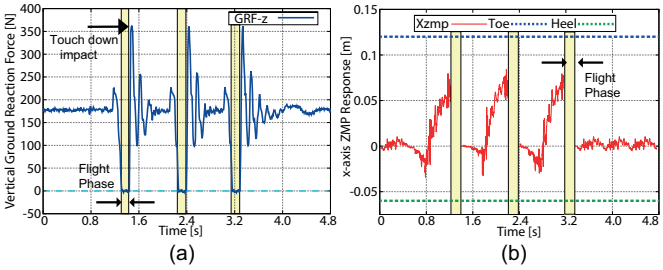

Fig. 7. a) Ground reaction force response. b) Measured ZMP response.

Finally, some significant moments from the resonant jumping experiment on our actual robot can be seen in Fig. 9. In this figure, it is possible to examine following moments. 1) Rest, 2) Lift-off, 3) Flight Phase, 4) Touch-down, 5) Landing. From 6 to 10, one may also observe the same moments for the second jump.

V. Conclusions and Future Work

To sum up, this paper presents a jumping pattern generation method that is applicable to bipedal robots with passive compliant joints. In the proposed method, there is no hardware-specific parameter for the pattern generation, so that it may be applicable to larger class of bipedal robots with passive compliance. Though we exploited the passive compliance in the joint level, one may use another elastic structure -such as a limb- as long as the identified resonance frequency is physically realizable. On the other hand, the passive compliance in the joint level has additional advantages in measuring and computing the deflection and elastic energy variations. Therefore, the performance evaluation can be realized in a relatively smoother manner.

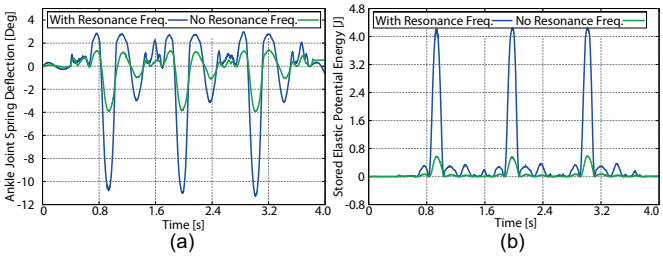

Fig. 8. Comparison between resonant (δ_1) and non-resonance ($\delta_1 + 0.25\delta_1$) jumping: a) Measured deflections, b) Stored Elastic Potential Energy.

Another prominent feature of the method is that the pattern generation algorithm is based on analytical functions. Moreover, initial conditions are tuned in a way to generate feasible jumping patterns, so that the method becomes systematic and easy-to-apply for real-time implementations.

Applying the presented technique, we conducted two legged jumping experiments on the actual compliant bipedal robot. In conclusion, we obtained repetitive, continuous and dynamically equilibrated jumping cycles with successful landing phases. Up to our knowledge, this paper presents one of a few jumping experiments through the utilization of resonance frequency and conducted on a fully actuated and passively compliant bipedal robot.

Recently, Paskevich and his colleagues revealed an analytical computation regarding the Cartesian stiffness matrix of passively compliant manipulators [23]. Authors believe that a possible extension of their work for floating-base robotic systems could be efficiently applied in our case. Therefore, in our next report, we are going to analyze the overall Cartesian stiffness matrix of our humanoid throughout jumping cycles. Efficient running motion through the exploitation of passive compliance will also be further investigated.

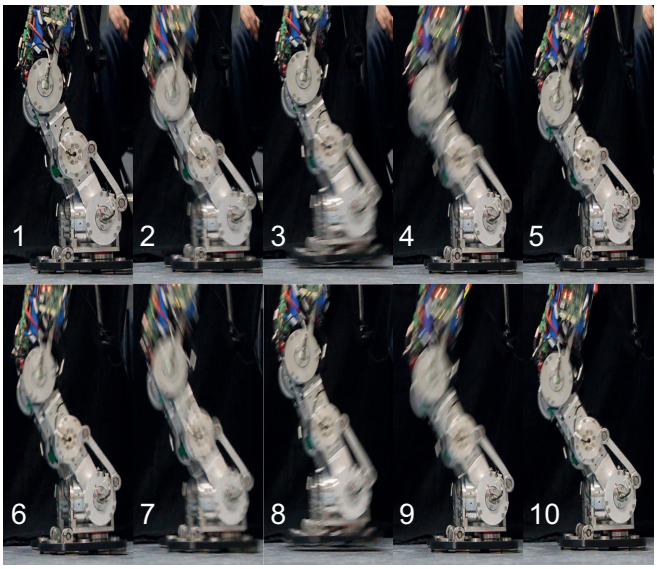

Fig. 9. Significant moments from jumping experiment at the resonance frequency: 1) Rest, 2) Lift-off, 3) Flight Phase, 4) Touch-down, 5) Landing. From 6 to 10, one may also observe the same moments for the second jump.

ACKNOWLEDGEMENTS

This work is supported by the European Commission FP7, "AMARSi" Project ICT-2009-4. Authors would like to thank Gianluca Pane, Phil Hudson and Stephen Morfey for their helpful assistance.

REFERENCES

[1] M. Zinn, O. Khatib, B. Roth, and J. K. Salisbury, "Playing it safe [human-friendly robots]," in *IEEE Robotics and Automation Magazine*, vol. 11, no. 1, 2004, pp. 12-21.

[2] T. J. Roberts, R. L. Marsh, P. G. Weyand and C. R. Taylor, "Muscular force in running turkeys: The economy of minimizing work," in *Science*, vol. 275, no. 5303, 1997, pp. 1113-1115.

[3] M. Ishikawa, P. V. Komi, M. J. Grey, V. Lepola and G. P. Bruggemann, "Muscle-tendon interaction and elastic energy usage in human walking," in *Journal of Applied Physiology*, vol. 99, no. 2, 2005, pp. 603-608.

[4] T. A. McMahon, and G. C. Cheng "The mechanics of running: How does stiffness couple with speed?," in *Journal of Biomechanics*, vol. 23, no. 1, 1990, pp. 65-78.

[5] R. Blickhan, "The spring-mass model for running and hopping," in *Journal of Biomechanics*, vol. 22, no. 11-12, 1989, pp. 1217-1227.

[6] S. Kajita, K. Kaneko, M. Morisawa, A. Nakaoka, and H. Hirukawa, "ZMP-based biped running enhanced by toe springs," in *Proc. IEEE Int. Conf. on Robotics and Automation*, Rome, Italy, 2007, pp. 3963-3969.

[7] B. Cho, J. Kim, and J. Oh, "Online balance controllers for a hopping and running humanoid robot," in *Advanced Robotics*, vol. 25, no. 9-10, 2011, pp. 1209-1225.

[8] T. Sugihara, and Y. Nakamura, "Enhancement of boundary condition relaxation method for 3D hopping motion planning of biped robots," in *Proc. IEEE Int. Conf. on Intelligent Robots and Systems*, San Diego, US, 2007, pp. 444-449.

[9] B. Ugurlu, and A. Kawamura, "ZMP-based online jumping trajectory generation for a one-legged robot," in *IEEE Transactions on Industrial Electronics*, vol.57, no.5, 2010, pp. 1701-1709.

[10] S. Sakka, and K. Yokoi, "Humanoid vertical jumping based on force feedback and inertial forces optimization," in *Proc. IEEE Int. Conf. on Robotics and Automation*, Barcelona, Spain, 2005, pp. 3752-3757.

[11] B. Vanderborght, R. Van Ham, B. Verrelst, M. Van Damme, and D. Lefeber, "Overview of the Lucy project: Dynamic stabilization of a biped powered by pneumatic artificial muscles," in *Advanced Robotics*, vol. 22, no. 10, 2008, pp. 1027-1051.

[12] K. Hosoda, T. Takuma, A. Nakamoto, and S. Hayashi, "Biped robot design by antagonistic pneumatic actuators for multi-modal locomotion," in *Robotics and Autonomous Systems*, vol. 56, no. 1, 2008, pp. 46-53.

[13] I. A. Anderson, I. A. Ieropoulos, T. McKay, B. O'Brein, and C. Melhuish, "Power for robotic artificial muscles," in *IEEE/ASME Transactions on Mechatronics*, vol. 16, no.1, 2011, pp. 107-111.

[14] B. Ugurlu, N. G. Tsagarakis, E. Spyrakos-Papastravridis, and D. G. Caldwell, "Compliant joint modification and real-time dynamic walking implementation on bipedal robot cCub," in *Proc. of IEEE Int. Conf. on Mechatronics*, Istanbul, Turkey, 2011, pp. 833-838.

[15] Adaptive Modular Architectures for Rich Motor Skills, EU supported FP7 Project, Online Available: http://www.amarsi-project.eu/ [Last Accessed: 5 Feb. 2012]

[16] F. Iida, J. Rummel, and A. Seyfarth, "Bipedal walking and running with compliant legs," in *Proc. IEEE Int. Conf. on Robotics and Automation*, Rome, Italy, 2007, pp. 3970-3975.

[17] J. Buchli, F. Iida, and A. J. Ijspeert, "Finding resonance: Adaptive frequency oscillators for dynamic legged locomotion," in *Proc. IEEE Int. Conf. on Intelligent Robots and Systems*, Beijing, China, 2006, pp. 3903-3909.

[18] N. G. Tsagarakis, Z. Li, J. A. Saglia, and D. G. Caldwell, "The design of lower body of the compliant humanoid robot "cCub"," in *Proc. IEEE Int. Conf. on Robotics and Automation*, Shangai, China, 2011, pp. 2035-2040.

[19] R. Caballero, M. A. Armada, and P. Alarcon, "Methodology for zero-moment point experimental modeling in the frequency domain," Journal of Vibration and Control, vol. 12, no. 12, pp. 1385-1406, 2006.

[20] A. Jafari, N. G. Tsagarakis, and D. G. Caldwell, "A novel intrinsically energy efficient actuator with adjustable stiffness (AwAs)," in *IEEE/ASME Transactions on Mechatronics*, Forthcoming paper.

[21] Y. Choi, D. Kim, Y. Oh, and B.-J. You, "Posture/walking control for humanoid robot based on kinematic resolution of CoM Jacobian with embedded motion," in *IEEE Transactions on Robotics*, vol. 23, no. 6, 2007, pp. 1285-1293.

[22] W. H. Press, S. A. Teukolsky, W. T. Vetterling, and B. P. Flannery, *Numerical Recipes in C: The Art of Scientific Computing* 2^{nd} *Edition*, Cambridge University Press, 1992.

[23] A. Pashkevich, A. Klimchik, S. Caro, and D. Chablat, "Cartesian stiffness matrix of manipulators with passive joints: Analytical approach," in *Proc. IEEE Int. Conf. on Intelligent Robots and Systems*, San Francisco, US, 2011, pp. 4034-4041.